gas isotopes, can be summarized as follows. The glass droplets from the bottom of core 74001/2 were produced, probably by lava fountaining, 3.63×10^9 years ago, a few tens of million years after the end of the lava flooding of Mare Serenitatis. Immediately or soon afterward, they were exposed to cosmic rays for about 38 million years. After this preexposure, the glass layer was completely shielded from cosmic rays by a layer several meters thick and was reexcavated by the impact that created Shorty Crater 17 million years ago. Since that time, the orange and black glasses remained undisturbed until collection.

O. EUGSTER
P. EBERHARDT
J. GEISS
N. GRÖGLER

Physikalisches Institut, University of Bern, 3012 Bern, Switzerland

References and Notes

1. J. S. Nagle, *Geochim. Cosmochim. Acta Suppl. 10* (1978), p. 1509; G. Heiken and D. S. McKay, *ibid.*, p. 1933.
2. G. Heiken, D. S. McKay, R. W. Brown, *Geochim. Cosmochim. Acta* **38**, 1703 (1974).
3. Results for the soils from other layers of the core and a discussion of other aspects were published in O. Eugster, P. Eberhardt, J. Geiss, N. Grögler, W. Kiesl, *Geochim. Cosmochim. Acta Suppl. 16* (1981), p. 541.
4. The trapped noble gases may have been incorporated into the sample by one or more of the following processes: implantation by solar wind irradiation, implantation of lunar atmospheric ions accelerated by the electric and magnetic fields generated by the solar wind, and adsorption of lunar atmospheric species with subsequent diffusion of gases into lunar material. In order to separate the components produced in situ from the trapped components five grain size fractions were prepared (approximate grain sizes $\geq$ 26, 17, 9, 3, and 1 μm) and for the fraction $\geq$ 26 μm noble gas extraction was performed in two temperature steps ($\leq$ 900°C and 900° to 1700°C). By these methods the concentrations and composition of the trapped component were determined [O. Eugster, N. Grögler, P. Eberhardt, J. Geiss, *Geochim. Cosmochim. Acta Suppl. 14* (1980), p. 1565]. Thus we were able to ensure that the fission xenon discussed in this report was produced from local uranium within the sample.
5. In the ^{39}Ar-^{40}Ar dating method a measured fraction of ^{39}K in the sample is converted to ^{39}Ar by neutron activation; the sample is then heated in stages to release this ^{39}Ar, together with radiogenic ^{40}Ar, by thermal diffusion. The argon is subsequently analyzed in a mass spectrometer. An ^{39}Ar-^{40}Ar age of 3.7×10^9 years for soil sample 74001,15 was given by P. Eberhardt, O. Eugster, J. Geiss, N. Grögler, M. Jungck, P. Maurer, M. Mörgeli, and A. Stettler [*Meteoritics* **10**, 93 (1975) (abstract)]. The age is recalculated in this report with constants given by R. H. Steiger and E. Jäger [*Earth Planet. Sci. Lett.* **36**, 359 (1977)].
6. J. C. Huneke, E. K. Jessberger, F. A. Podosek, G. J. Wasserburg, *Geochim. Cosmochim. Acta Suppl. 4* (1973), p. 1725; L. E. Nyquist, B. M. Bansal, H. Wiesmann, B. M. Jahn, *ibid. Suppl. 5* (1974), p. 1515.
7. W. Kiesl, private communication.
8. D. S. Woolum and D. S. Burnett, *Earth Planet. Sci. Lett.* **21**, 153 (1974).
9. E. K. Hyde, *The Nuclear Properties of the Heavy Elements* (Prentice-Hall, Englewood Cliffs, N.J., 1964), vol 3.
10. R. C. Reedy, *Geochim. Cosmochim. Acta Suppl. 16* (1981), p. 1089.
11. O. Eugster, P. Eberhardt, J. Geiss, N. Grögler, M. Jungck, M. Mörgeli, *ibid. Suppl. 8* (1977), p. 3059.
12. We thank E. Anders for valuable suggestions and criticisms, A. Schaller and U. Bütikofer for technical assistance, and L. Reichert and R. Wright for preparation of the manuscript. Supported by Swiss National Science Foundation grants NF 2.180.78 and 2.467.79.

24 May 1982; revised 1 September 1982

Crystalline Todorokite Associated with Biogenic Debris in Manganese Nodules

Abstract. *Platy intergrowths of crystalline todorokite are associated with biogenic debris in the cores of manganese nodules from a site in the Pacific Ocean. Analyses by electron diffraction and transmission electron microscopy demonstrate that this material is composed of tunnels of chains of linked MnO_6 octahedra. The chemical composition, morphology, and stability of the todorokite differ from those of nickel- and copper-rich manganese oxides in nodules that have been identified as todorokite or buserite in earlier investigations.*

The identities and structures of manganese oxyhydroxide phases in marine manganese nodules have been debated extensively for more than three decades (*1*). The phases are cryptocrystalline and intergrown on a microscopic scale with iron oxyhydroxides, biogenic debris, and aluminosilicate grains. The lack of suitable homogeneous samples has severely hampered mineralogical studies and structural interpretation. A question of particular interest is the identity of the host phase and the structural sites of copper and nickel in manganese nodules. X-ray diffraction patterns of this phase characteristically contain reflections at approximately 9.6, 4.8, 3.2, and 2.4 Å. This material, which we call a "10-Å phase," has been compared to both todorokite (*1, 2*), a tektomanganate, and buserite, a phyllomanganate (*3*).

Recently, Chukhrov *et al.* (*4*) presented electron diffraction data and transmission electron micrographs of crystalline todorokite with $a_0 = 14.6$ Å from the core of a Pacific Basin nodule. Siegel (*5, 6*) identified fibrous todorokite with $a_0 = 9.8$ Å in the cores of manganese nodules by scanning electron microscopy and electron diffraction. Recently, Turner *et al.* have shown by means of structural imaging with high-resolution transmission electron microscopy that the structure of this material is the same as that of samples of todorokite from terrestrial locales (*7, 8*). The purpose of this report is to describe the chemistry, morphology, and geological occurrence of crystalline todorokite associated with biogenic debris in nodules from the north equatorial Pacific Ocean.

The samples were taken from free-fall grabs at station 19 of the Manganese Nodule Program BOMDROP cruise MN75-03. This station is centered at approximately 140°W, 11°N and includes Site S of the present Manganese Nodule Project (MANOP). The geology of this site has been described in (*6, 9*). Nodules containing cores composed of crystalline todorokite are found almost exclusively in free-fall grabs located near the base of a series of fault scarps where indurated carbonate sediment is exposed. Nodules in which the crystalline todorokite was found are small (average diameter, 1.6 cm), are spheroidal or polyspheroidal in shape, and have smooth surface textures.

A polished cross section of a nodule from free-fall grab MN75-03-FFG001 is shown in Fig. 1a. The crystalline oxide core is more highly reflective and homogeneous than the mottled and laminated zones of the outer layers of the nodule. Partial chemical compositions obtained from quantitative microprobe analyses of the core and outer layers are shown in Table 1 (*10*). The presence of todorokite in the nodule cores was initially determined by x-ray powder diffraction studies. An orthorhombic unit cell with lattice constants of $a_0 = 9.82$ Å, $b_0 = 2.89$ Å, and $c_0 = 9.59$ Å was calculated with a least-squares refinement of the positions of 14 reflections (*11*).

Scanning electron micrographs (*5, 6*) show that these cores are composed almost entirely of molds of biogenic debris (Fig. 1b). Well-preserved molds of discoasters and coccoliths are common, and impressions of Radiolaria also occur. Element mapping by energy-dispersive analysis of emitted x-rays (*5, 6*) showed that the material is almost entirely manganese oxide; very little of the biogenic SiO_2 or $CaCO_3$ remains. Needles of manganese oxide and platy intergrowths with pseudohexagonal symmetry are shown in Fig. 1c. Transmission electron micrographs (*12*) show that the bulk of the material within these nodule cores is composed of plates with fine-scale hexagonal trillings (Fig. 1d). Selected-area electron diffraction patterns

obtained from this material (Fig. 1e) are similar to those obtained from samples of terrestrial todorokite (*2*, *4*). The high degree of ordering of the trigonal twinning contributes to the strong hexagonal reflections of the pattern produced by the superposition of three reciprocal lattices rotated 120° relative to one another. A high-resolution structural image of the todorokite in the nodule cores is shown in Fig. 1f. In this photograph almost all the todorokite fibers are oriented perpendicular to the electron beam direction. Widths of double through septuple chains of MnO_6 octahedra can be observed. Triple chains predominate (Fig. 1f), leading to the characteristic a_0 spacing of about 9.6 Å.

We observed several physical and chemical characteristics of the marine todorokite that may be significant in understanding the paragenesis of this mineral. The chemical composition and physical properties of the todorokite in the nodule nuclei differ from those of a 10-Å phase in the nickel- and copper-rich outer layers of the nodule. In Table 1 the composition of the todorokite core is compared to that of layers of a manganese oxide that is similar in appearance and composition to the 10-Å phase described in (*1*, *13*, *14*). Relative to the other 10-Å phase, the todorokite contains higher concentrations of manganese, barium, and potassium; lower concentrations of iron and copper; and much smaller amounts of nickel.

Table 1. Partial electron microprobe analyses of todorokite cores and other manganese oxide layers (oxide weight percentages).

Oxide	Todorokite*	10-Å phase†
MnO_2	74.0	66.2
NiO	0.2	3.8
CuO	1.5	2.8
CaO	0.6	1.7
MgO	3.0	4.9
$Al_2O_3 + SiO_2$	2.8	8.5
BaO	1.3	0.2

*Mean of 23 analyses from todorokite in area 3 of Fig. 1a. †Mean of 20 analyses from layers containing a 10-Å phase in areas 1 and 2 in Fig. 1a.

We were unable to identify todorokite in the outer layers of the nodule. Many workers have reported that the 10-Å phase in nodules dehydrates in a vacuum or air to birnessite or vernadite (*1*, *4*, *13*). We have observed that, although this transformation occurs for the 10-Å phase in the outer layers, the todorokite in the nodule nuclei is stable in a vacuum and under an electron beam. Samples stored in a desiccator for several years did not dehydrate. The enhanced stability of the todorokite in the core relative to that of the 10-Å phase in the outer layers may be related to the higher concentrations of the large cations barium and potassium in the sites within the tunnels of the todorokite structure. High concentrations of these cations stabilize manganese oxides with tunnel structures such as hollandite and romanéchite relative to phases with other structure types (*15*). Chukhrov *et. al.* (*4*) and Turner and Buseck (*8*) have observed todorokite intergrowths with a variety of tunnel dimensions. Intergrowths from different chemical environments may have different predominant tunnel sizes. The presence of locally high concentrations of potassium or barium in seawater may favor the formation of tunnels with

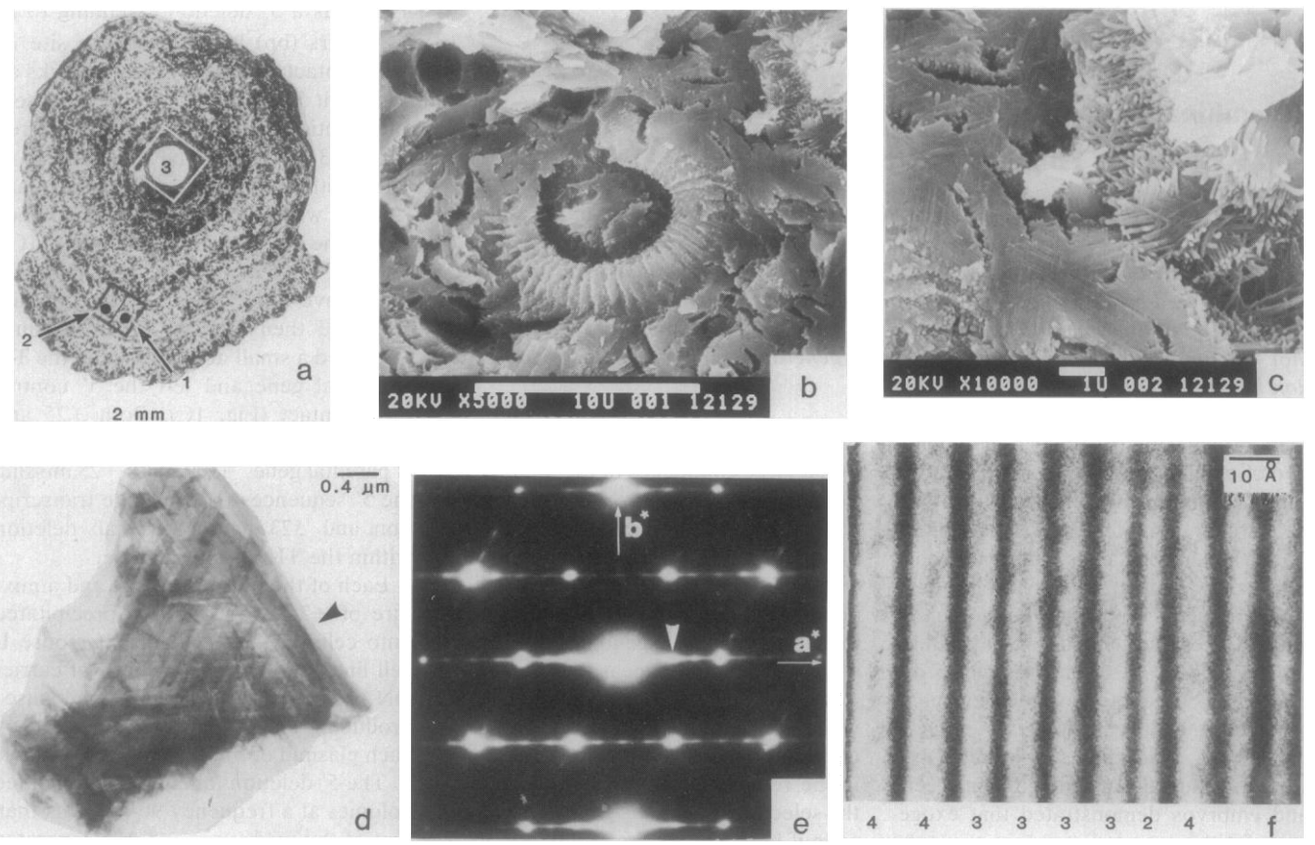

Fig. 1. (a) Polished cross section of a nodule (MN75-03-001-23B) with a core of crystalline todorokite (area 3). (b) Mold of coccolith shield and surrounding material composed of intergrowths of todorokite needles in the nodule core. (c) Close-up of todorokite needles and platy intergrowths. (d) Transmission electron micrograph of a plate of twinned todorokite. (e) Selected-area diffraction pattern of a plate of twinned todorokite. The arrow marks the maximum at 4.8 $Å^{-1}$. The streaking along the $\vec{a}^*$ direction indicates disorder at distances greater than 4.8 Å along $\vec{a}$. (f) High-resolution transmission electron micrograph of marine todorokite from the area indicated in (d). Chains of different widths are marked; triple chains are the most common unit.

smaller dimensions relative to larger, less stable tunnels or sheet structures. Further examination of marine and terrestrial todorokite by high-resolution imaging and concurrent chemical microanalysis is necessary to determine if a relationship exists between chemical composition and tunnel dimensions.

MALCOLM D. SIEGEL
Organization 9413,
Sandia National Laboratories,
Albuquerque, New Mexico 87185
SHIRLEY TURNER
Department of Geology,
Arizona State University, Tempe 85287

References and Notes

1. R. G. Burns and V. M. Burns, in *Marine Manganese Deposits*, G. P. Glasby, Ed. (Elsevier, Amsterdam, 1977), pp. 185–248; *Scanning Electron Microsc.* **1**, 245 (1978).
2. J. A. Straczek, A. Horen, M. Ross, C. M. Warshaw, *Am. Mineral.* **45**, 1174 (1960); F. T. Manheim, in *Symposium on Marine Chemistry*, D. R. Schink and J. T. Corliss, Eds. (Occasional Publication, University of Rhode Island, 1965), vol. 3, pp. 217–276.
3. W. Buser and A. Grutter, *Schweiz. Mineral. Petrog. Mitt.* **36**, 49 (1956); R. Giovanoli, W. Feitknecht, F. Fischer, *Helv. Chim. Acta* **54**, 1112 (1971).
4. F. V. Chukhrov *et al.*, *Nature (London)* **278**, 631 (1979); *Int. Geol. Rev.* **22**, 75 (1980).
5. M. D. Siegel, *Geol. Soc. Am. Abstr. Programs* **11**, 516 (1979).
6. _____, thesis, Harvard University (1981).
7. S. Turner, M. D. Siegel, P. R. Buseck, *Eos* **62**, 306 (1981); *Nature (London)* **296**, 841 (1982).
8. S. Turner and P. R. Buseck, *Science* **212**, 1024 (1981).
9. M. Karas, thesis, Scripps Institution of Oceanography (1978).
10. Quantitative point analyses for 17 elements were obtained at the Department of Geological Sciences, Harvard University, with an automated Applied Research Laboratories EMX-SM electron microprobe and the correction method outlined by A. Bence and A. Albee [*J. Geol.* **76**, 322 (1968)] and A. Albee and L. Ray [*Anal. Chem.* **42**, 1408 (1970)].
11. Debye-Scherrer x-ray diffraction patterns were obtained with manganese-filtered Fe Kα radiation. The least-squares refinement of the unit cell parameters was calculated with the use of LCLSQ, a program written by C. W. Burnham, Department of Geological Sciences, Harvard University.
12. Samples of nodule cores were ground to a fine powder under water, suspended in water, and applied to a carbon film supported by a 200-mesh grid. Electron diffraction patterns and structural images of this material were obtained in a slightly modified JEOL JEM 100B microscope [D. R. Veblen and P. R. Buseck, *Am. Mineral.* **64**, 687 (1979)].
13. A. Usui, thesis, University of Tokyo (1979).
14. P. Halbach and M. Ozkara, in *La genèse des nodules manganese* (No. 289, Collection Internationale du Centre National de la Recherche Scientifique, Paris, 1979), pp. 77–88.
15. A. Bystrom and A. M. Bystrom, *Acta Crystallogr.* **3**, 146 (1950).
16. We are grateful to K. Jones, M. Carpenter, and E. Seeling for their assistance with the electron microscopy. Samples were provided from the MANOP nodule collection by T. Walsh. We thank H. D. Holland, P. Buseck, and R. Burns for their guidance and support of this research. This work was supported by grants EAR79-26375 and EAR79-04364 from the Earth Sciences Division of the National Science Foundation (NSF) and grant 832550CE from the NSF International Decade of Oceanographic Exploration Manganese Nodule Program.

5 May 1982; revised 17 August 1982

Recombination During Gene Transfer into Mouse Cells Can Restore the Function of Deleted Genes

Abstract. *Two plasmids containing nonoverlapping deletions of the herpes simplex virus thymidine kinase gene were introduced into thymidine kinase–deficient mouse L cells by DNA-mediated gene transfer. Thymidine kinase–producing transformants were generated by a mixture of the two plasmids at a frequency significantly greater than that generated by either plasmid alone. Southern blot analyses demonstrated that functional thymidine kinase genes were generated by homologous recombination between the two deletion mutants.*

In prokaryotic systems, the integration of exogenously added DNA into the genome of recipient cells occurs primarily through homologous recombination (*1*). In eukaryotic cells, integration has been studied most extensively in yeast, where it occurs both at sites of homology and at sites not linked to the cellular homolog (*2–4*). In some cases, genes are integrated by double crossover events to replace the cellular gene (*4*).

Previous experiments in which DNA was introduced into mammalian cells and embryos demonstrated that exogenous DNA integrated at many sites in the genome (*5–9*), so that the integrations appeared random. An apparent absence of homologous recombination might be explained by several hypotheses.

1) In experiments in which calcium phosphate was coprecipitated with DNA, large complexes of the input DNA (termed pekelasomes or transgenomes) were found in the recipient cell (*5, 8, 9*). Since most transfer experiments include whole cell DNA either as a carrier or donor, integration at sites homologous to the DNA in the transgenome could occur at many sites and appear random.

2) In many systems, including the widely used thymidine kinase (TK) gene of herpes simplex virus (HSV), no DNA in the recipient cell was homologous to the selected exogenous gene. Therefore, even if homologous recombination were possible, it would not have been detected.

3) The mammalian genome is 750 times larger than the *Escherichia coli* genome (*10*), so that even if a homologous gene were the most common integration site, the sum of integration events at sites of partial or no homology might be greater.

Sister chromatid exchange, meiotic recombination, immunoglobulin gene rearrangements (*11–13*), and the demonstration of recombination between SV40 molecules (*14*) suggest that the machinery necessary for homologous recombination is present in mammalian cells. Recombination between independent molecules has been detected during gene transfer (*15*), but previous experiments did not distinguish between random and homologous recombination. We now describe experiments designed to determine whether homologous recombination could occur between two plasmids containing nonoverlapping deletions in the TK gene during DNA-mediated gene transfer.

Two deletion mutants of the HSV TK gene were cloned into the plasmid pBR322 (see Fig. 1C). The functionally wild-type plasmid, pTK−109 (referred to herein as −109), contains a 1.7 kilobase pair (kbp) fragment of HSV DNA that includes an intact structural TK gene and its 5′ control region. One deletion mutant, pTK+25 (herein referred to as +25), has a 5′ deletion extending to 25 base pairs (bp) beyond the cap site. It has an intact structural gene but lacks all important 5′ control sites (*16*). The second deletion mutant, pTKΔ23 (referred to as Δ23) was prepared by digestion of −109 with the restriction endonuclease Kpn I, which cuts the plasmid once within the TK structural gene (Fig. 1C). The DNA was digested with S1 nuclease to remove the 4-base single-stranded ends and then ligated. This procedure generated a small deletion within the TK structural gene and left the 5′ control region intact (Fig. 1C). Both +25 and Δ23 are deletion mutants of the functional parental gene, −109, with +25 missing the 5′ sequences that regulate transcription and Δ23 having a small deletion within the TK structural gene.

Each of the plasmids alone and a mixture of +25 and Δ23 were precipitated onto cells of the TK-deficient mouse L cell line, Ltk^-, in the absence of carrier DNA. The number of thymidine kinase–producing (TK^+) colonies generated by each plasmid or mixture is given in Table 1. The 5′ deletion mutant +25 generated colonies at a frequency 90-fold less than that of the wild type, and Δ23 generated no colonies in any experiments. The mixture of +25 and Δ23 generated colonies at a frequency ninefold lower than that of the wild-type control and tenfold higher than that of +25 alone.